Field investigation and analysis of rockburst and spalling in a deep hard-rock mine

Xiao Peng
Central South University
Zhao Guoyan (gyzhao@csu.edu.cn)
Central South University
Liu Huanxin
Shandong Gold Group

Research Article

Keywords: Deep hard-rock mine, Ground pressure disasters, Strain energy release, Rockburst, Spalling, Maximum tangential stress

Posted Date: February 17th, 2021

DOI: https://doi.org/10.21203/rs.3.rs-197278/v1

Field investigation and analysis of rockburst and spalling in a deep hard-rock mine

Xiao Peng [1], Zhao Guoyan [1*], Liu Huanxin [2]

[1] *School of Resources and Safety Engineering, Central South University, Changsha 410083, China*

[2] *Deep Mining Laboratory of Shandong Gold Group, Laizhou 261442, China*

Abstract

In order to investigate the ground pressure disasters in deep hard-rock mines, field investigation and theoretical analysis were carried out in a deep hard-rock mine. It is found that the degree and number of ground pressure disasters in the mine have increased significantly with depth. When the maximum tangential stress between 0.4-0.6 times the uniaxial compressive strength of surrounding rock, surrounding rock is prone to local spalling. When maximum tangential stress is greater than 0.6 times uniaxial compressive strength, serious failure is easy to occur, such as rockbursts and large-area collapses. After excavation, the rebound strain and displacement of surrounding rock increases linearly with buried depth, and the strain energy released of surrounding rock increases rapidly with the second power of buried depth. The rapidly increasing strain energy is main reason why deep ground pressure disasters in the mine are becoming more and more serious. In terms of surrounding rock support, energy-absorbing materials such as energy-absorbing bolts can well absorb strain energy released by surrounding rock. The energy-absorbing bolts are used for design of roadway support in the mine.

Keywords:

Deep hard-rock mine; Ground pressure disasters; Strain energy release; Rockburst; Spalling; Maximum tangential stress

1. Introduction

With the decrease of shallow mineral resources and the increase in human demand, deep resource exploitation is now very common. At present, there are 112 metal mines in the world with mining depths below 1000m [1]. However, in deep hard-rock mines, more and more disaster phenomena that are not available in shallow part have occurred, such as rockburst, large-scale collapse, rock spalling, and core disking. Obviously these disasters are directly related to the high

* Corresponding author.
E-mail address: gyzhao@csu.edu.cn (G. Zhao)

ground stress in deep mines.

In response to deep mines disasters, scholars have carried out a lot of work from the aspects of mechanism research, surrounding rock support, and disaster prediction. The mechanism research includes in-situ stress measurement [2-4], surrounding rock quality classification [5-7], rock mechanics test [8-11], various failure criteria [12-14], et al. The surrounding rock support includes the use of new-type bolts [15-18], filling of goaf [19-22], and combination of multiple support methods [23-25], and so on. Disaster prediction includes microseismic monitoring [26-28], various rockburst prediction models [29-31], et al.

Although a lot of researches has been invested in deep mines and many research results have been obtained, the problem of deep mines disasters has not yet been well resolved. The rockburst, large-scale collapse, spalling, floor bulge and other phenomena still occurred frequently in deep mines. Support failures often occur in disaster locations. Disaster prediction methods have the problems of low accuracy and timeliness, and are difficult to avoid disasters. The frequent ground pressure disasters still bring huge challenges to personnel's lives and company operation.

In terms of the mechanism of ground pressure disasters in deep mines, many studies only consider the stress concentration caused by high ground stress and excavation space, which is relatively one-sided. Although some studies can reproduce the spalling process of surrounding rock through laboratory test and numerical simulation, the boundary stress imposed by it is far greater than the actual ground stress of rock engineering. For example, in actual deep hard-rock mines, when buried depth is 800m, surrounding rock is prone to spalling, and the vertical principal stress is about 22MPa. Taking a laboratory true triaxial test as an example [32], the externally applied vertical principal stress reached 150 MPa when specimen with a hole occurs spalling, which was 7 times the actual ground stress. This shows that the spalling and failure phenomenon of surrounding rock in deep mines needs more complete research and explanation.

In deep hard-rock mines, not only should the stress concentration after excavation be considered, but also the strain energy release of surrounding rock after excavation should be considered. Before excavation of deep hard-rock mines, surrounding rock was in a state of compressive stress. After excavation, a free surface appeared in surrounding rock. The stress on free surface side of surrounding rock suddenly drops to 0, surrounding rock will move to free surface and release the compressive strain energy. This caused roof moves down, floor bulges, and sidewalls deform after

excavation. It is also one of energy sources for failure of surrounding rock.

Therefore, based on field investigation of ground pressure disasters in a deep hard-rock mines, this research conducts theoretical analysis from three aspects of stress concentration, strain rebound and strain energy release after excavation. The research shows current situation of ground pressure disasters in deep hard-rock mines, and makes reasonable explanations for ground pressure disasters of different buried depths in the mine.

2. Investigation of ground pressure disasters in a deep hard-rock mine

2.1. Brief introduction of the mine

The Xincheng Gold Mine is located in Laizhou City, Shandong Province, China, adjacent to the Bohai Sea, with geographic coordinates of 119°57′ east longitude and 37°24′ north latitude. The average elevation of mining area is 30m, and the average inclination of ore body is about 30°. At present, mining depth of the mine has reached -1080m, which is a typical deep mine.

The ore body is mainly pyrite sericite, and surrounding rock is mainly sericitized granodiorite. The average uniaxial compressive strength of surrounding rock is about 150.5MPa, average tensile strength is about 12.1MPa, and average elastic modulus is about 35.7GPa, which belongs to hard rock.

2.2. Investigation results of ground pressure disaster

In order to study deep ground pressure disasters at the mine, an in-site investigation was carried out in 2020. Investigation methods include consulting mine technicians and engineering field investigations. The ground pressure disasters of different buried depths are shown in Table 1 and Figs. 1-4.

The main ground pressure disasters of the mine include spalling in roof and sidewall, rock bolt falling off, rockburst, and large-area of collapse. The slabbing of surrounding rock starts from buried depth of 745m, the spalling of surrounding rock and rock bolt fall off occurred from buried depth of 830m, the rockburst and large-area of collapse start from buried depth of 980m. The phenomenon of different depths shows that the severity of ground pressure disasters increases significantly with depth.

In terms of the location of ground pressure disaster, rockburst and spalling mostly occur in the horizontal sidewall and excavation face, while the roof in vertical direction has less rockburst and spalling. The in-situ stress test results show that the maximum horizontal principal stress is greater than the vertical principal stress. This means that the number of rockburst and spalling parallel to the maximum horizontal principal stress direction is larger than that perpendicular to the maximum horizontal principal stress direction.

Table 1. Ground pressure disaster survey of Xincheng Gold Mine in 2020

Buried depth/ m	Related ground pressure disaster phenomenon (partial area)
745	Surrounding rock of roadway is broken, and there are obvious joints and cracks, as show in Fig. 1
830	Surrounding rock is broken, roof spalling and slabbing are common in roadways, which cause rock bolts falling off, as show in Fig. 2
930	Roof of roadway spalling and fragmentation are common, and roadway deformation is large. As shown in Fig. 3, roof of stope has pumice stones, and surrounding rocks on both sides are relatively broken. There are many obvious joint cracks on roof and both sides
980	A rockburst occurred during construction of a cutting lane in a stope, ore ejected from excavation face. Spalling occured on both sidewalls of surrounding rocks after rockburst. Exploded rocks are uniform and small in size, as shown in Fig. 4. A rockburst occurred when the first layer was mined in a stope, and a large amount of rock was ejected. A rockburst occurred in cutting roadway, and rock on one sidewall ejected out in flakes. Surrounding rock often produces rumbling sound when drilling rock.
1015	In 2019, there was a large-area of collapse at location of three fork of a roadway, with an area of about 20 square meters
1080	In 2020, there was a large-area of collapse under pass of blind inclined shaft, and all supporting bodies were destroyed

Fig. 1 Mining depth 745m

Fig. 2 Mining depth 830m

Fig. 3 Mining depth 930m

Fig. 4 Mining depth 980m

2.3. Quality evaluation of surrounding rock in the mine

In order to evaluate surrounding rock conditions in the mine, RQD and K_v values of the surrounding rock were measured. K_v is rock mass integrity coefficient, which reflects integrity of engineering rock mass, and is calculated by Eq. (1).

$$K_v = \left[c_{pm} / c_{pr}\right]^2 \tag{1}$$

Where c_{pm} is rock mass elastic longitudinal wave velocity (m/s), c_{pr} is rock elastic longitudinal wave velocity (m/s).

RQD and K_v values of surrounding rocks at different depths are shown in Table 2 and Fig. 5. A strong rockburst grade line (RQD>0.7) and a relatively complete rock mass line (K_v>0.55) are added in Fig. 5. It can be seen from Fig. 5 that integrity of the surrounding rocks is relatively good, and it is easy to accumulate elastic energy, which is conducive to occurrence of rockburst. The investigation results in Table 1 also show that surrounding rock of the mine in deep is prone to rockburst.

Table 2. RQD and K_v value of surrounding rock at different buried depth

Buried depth	RQD	K_v
950m	0.80	0.93
1050m	0.60	0.61
1150m	0.86	0.81
1250m	0.83	0.89
1350m	0.84	0.95

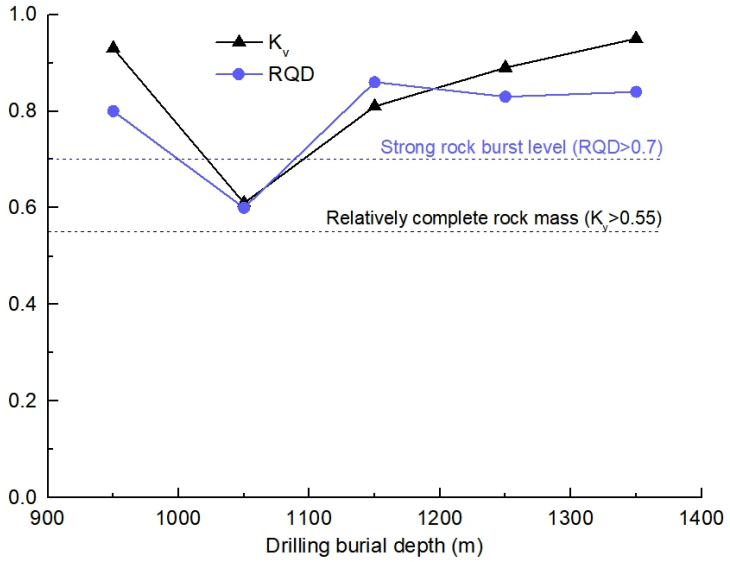

Fig. 5 RQD and K_v values of surrounding rock at different buried depths of the mine

3. Analysis of ground pressure disasters in the mine

3.1. Maximum tangential stress after excavation

In order to obtain distribution law of in-situ stress field in the mine, the hole wall strain relief method is used to measure in-situ stress. The test results of principal stress in three directions are shown in Eq. (2). The azimuth angle of maximum horizontal principal stress is between 260° and 285°, and the direction is nearly approximately perpendicular to the ore body. The effective range of

the Eq. (2) is about from 500m to 1300m buried depth.

$$\begin{cases} \sigma_H = 0.0461h - 7.11 \\ \sigma_h = 0.0294h - 9.34 \\ \sigma_v = 0.0266h \end{cases} \tag{2}$$

Where σ_H is maximum horizontal principal stress (MPa), σ_h is minimum horizontal principal stress (MPa), σ_v is vertical principal stress (MPa), h is buried depth (m).

Stress state of the mine's horizontal transportation roadway is shown in Fig. 6. Considering stress concentration, Eq. (3) is used to calculate the maximum tangential stress in roof and excavation surface of roadway. The maximum tangential stresses are shown in Eq. (4) and Fig. 7.

Some studies shown that when maximum tangential stress of surrounding rock between 0.4-0.6 times uniaxial compressive strength (UCS) of surrounding rock, surrounding rock is prone to spalling [33-35]. The failure behavior of the mine roadway in range of 0.4-0.6 times UCS in Fig. 7 also proves this point of view. In addition, it is worth adding that when maximum tangential stress of surrounding rock exceeds 0.6 times UCS, surrounding rock of the mine will suffer more serious failure, such as rockbursts and large-scale collapse.

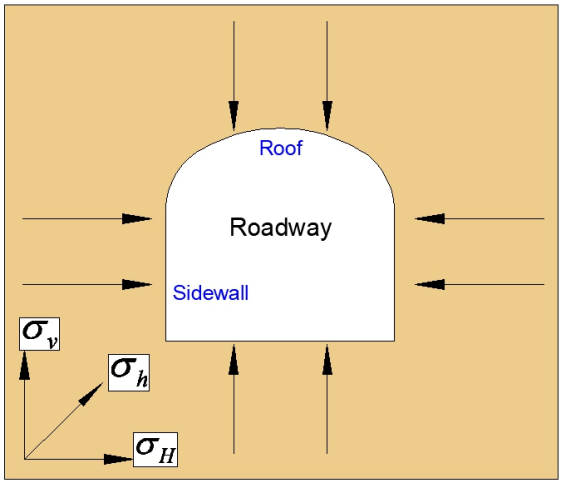

Fig. 6 Stress state of the horizontal transportation roadway

$$\begin{cases} \sigma_{\text{Roof}} = 3\sigma_{\text{H}} - \sigma_{\text{v}} \\ \sigma_{\text{Excava-face}} = 3\sigma_{\text{H}} - \sigma_{\text{h}} \end{cases} \tag{3}$$

$$\begin{cases} \sigma_{\text{Roof}} = 0.1117h - 21.33 \\ \sigma_{\text{Excava-face}} = 0.1089h - 11.99 \end{cases} \tag{4}$$

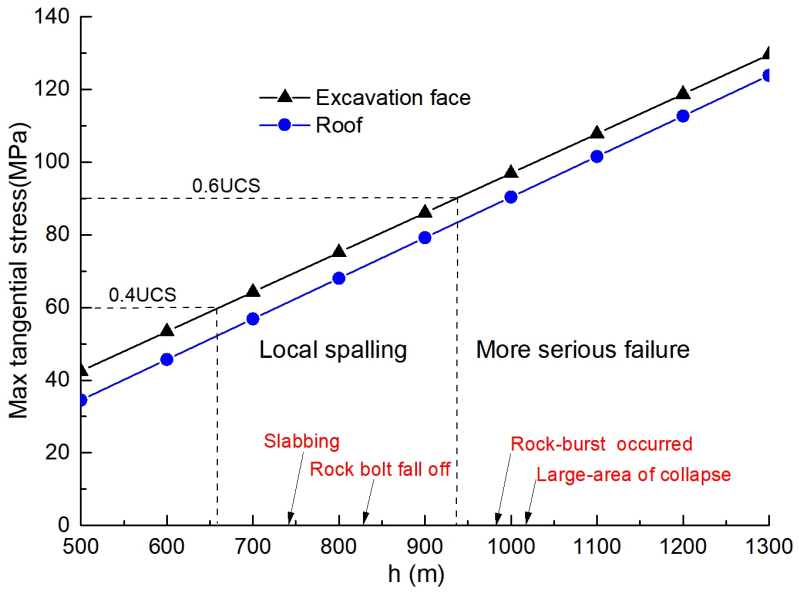

Fig. 7 Maximum tangential stress of roadways at different buried depth

3.2. Strain rebound and displacement after excavation

As shown in Fig. 8, the elastomer undergo a compressive strain of ε_C under action of compressive stress σ. When compressive stress on right of elastomer suddenly disappears, the right of elastomer will first return to stress-free position. Due to speed inertia, the rebound will continue to produce a tensile strain ε_T. It is easy to know that ε_C is equal to the ratio of stress σ to elastic modulus *E*, and ε_T is equal to ε_C, as shown in Eq. (5). It can be seen from Fig. 8 that maximum strain during rebound process is $\varepsilon_C + \varepsilon_T$, which is $2\sigma/E$.

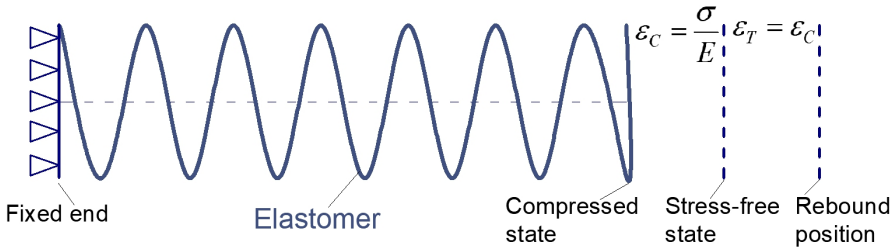

Fig. 8 Strain rebound process of elastomer after stress relief

$$\begin{cases} \varepsilon_C = \sigma/E \\ \varepsilon_T = \varepsilon_C \end{cases} \tag{5}$$

Therefore, after deep roadway is excavated, surrounding rock will also undergo the strain rebound due to appearance of free surface. Rock is an elastoplastic material and its rebound strain is

smaller than that of elastic body. The strain recovery coefficient of rock k_1 can be introduced into calculation, and the value of k_1 is obtained from uniaxial loading and unloading test of surrounding rock. The rebounded strain of roof, sidewalls and excavation surface of roadway in the mine is calculated by Eq. (6). Substituting values of each parameter into Eq. (6), rebounded strain of roof, sidewalls, and excavation surface is shown in Eq. (7) and Fig. 9.

$$\begin{cases} \varepsilon_{Roof} = k_1 \dfrac{2\sigma_v}{E} \\ \varepsilon_{Sidewall} = k_1 \dfrac{2\sigma_H}{E} \\ \varepsilon_{Excava-face} = k_1 \dfrac{2\sigma_h}{E} \end{cases} \tag{6}$$

Where k_1 is strain recovery coefficient of rock and is about 0.87, E is elastic modulus and is 35.7 GPa.

$$\begin{cases} \varepsilon_{Roof} = 4.87(0.0266h) \times 10^{-5} \\ \varepsilon_{Sidewall} = 4.87(0.0461h - 7.11) \times 10^{-5} \\ \varepsilon_{Excava-face} = 4.87(0.0294h - 9.34) \times 10^{-5} \end{cases} \tag{7}$$

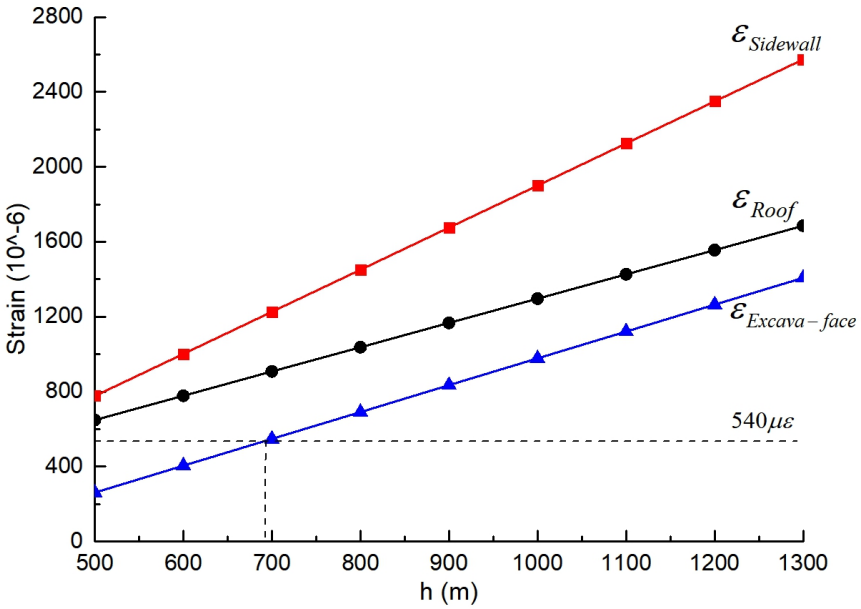

Fig. 9 Rebounded strain of sidewall, roof and excavation surface of roadway at different buried depths

The maximum tensile strain of hard rock under direct tension test is about $270\mu\varepsilon$ [36]. It can be seen from Fig. 8 that the total strain during rebound process is twice the tensile strain. Therefore, tensile cracks may occur when rebounded strain of surrounding rock is greater than $540\mu\varepsilon$. It can

be seen from Fig. 9 that rebounded strain of surrounding rock in the mine is relatively large, which easily leads to large deformation and tensile failure of surrounding rock. In addition, due to the restraint effect of surrounding rock, cracks may not occur where rebounded strain is relatively small.

The influence range of excavation on surrounding rock is about three times of roadway span. It is known that the width of transportation roadway in the mine is 4.5m, then the influence range of sidewall is 13.5m, and the displacement of sidewall is about 13.5m times the rebounded strain. Through calculation, the displacement of sidewall at depth of 1000m is 25.6mm, which is small compared with the size of roadway. However, in the soft rock roadway with small elastic modulus, it can be known from Eq. (6) that the rebounded strain will be large. If the elastic modulus of soft rock is 0.2 times that of the hard rock, the displacement of soft surrounding rock will reach 128mm, which is the reason why the soft rock roadway is prone to large deformation, as shown in Fig. 10.

Fig. 10 Large deformation of sidewall in a soft rock roadway

3.3. Strain energy released after excavation

The strain rebound after excavation is accompanied by release of strain energy, so it is necessary to calculate the amount of strain energy released after excavation.

As shown in Fig. 11, an elastic plate is subjected to uniformly distributed stress σ. Cutting a crack with area A in middle will cause release of strain energy on both sides of the crack. From the knowledge of fracture mechanics, it can be known that the released strain energy U_e is calculated

by Eq. (8).

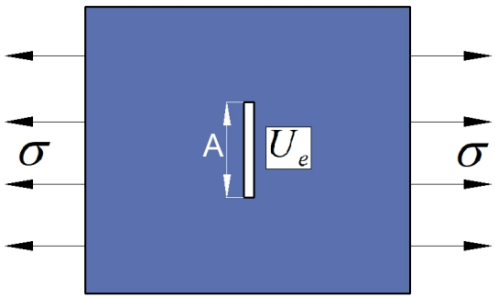

Fig. 11 The elastic plate subjected to uniform stress is cut with a crack with area A

$$U_e = \frac{\pi \sigma^2 A^2}{4E} \tag{8}$$

Deep rock mass is in a state of high ground stress compression, and roadway excavation will also cause release of strain energy. In order to facilitate calculation, cross section of the roadway is simplified as a rectangle, as shown in Fig. 12. $U_{e\text{-}Roof}$ represents the strain energy released by roof, and $U_{e\text{-}Sidewall}$ represents the strain energy released by sidewall. The roof in Fig. 12 is equivalent to one side of the crack in Fig. 11, so the strain energy released $U_{e\text{-}Roof}$ by roof is half of U_e. Besides, because rock is an elastoplastic body, strain energy released during unloading is often less than the energy inputted by loading. The energy release coefficient of rock k_2 can be introduced in calculation, and k_2 is determined by uniaxial loading and unloading test of surrounding rock. The strain energy released by roof and sidewall in the mine is calculated by Eq. (9).

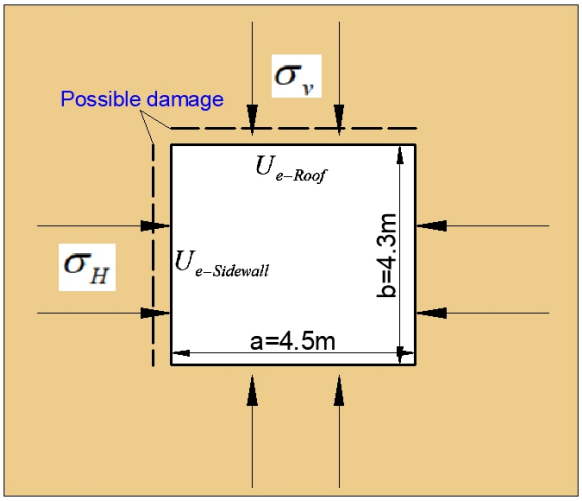

Fig. 12 Strain energy released after roadway excavation and possible damage

$$\begin{cases} U_{e-Roof} = k_2 \dfrac{\pi \sigma_v^{\,2} a^2}{8E} \\ U_{e-Sidewall} = k_2 \dfrac{\pi \sigma_H^{\,2} b^2}{8E} \end{cases} \tag{9}$$

Where a is 4.5m, b is 4.3m, k_2 is about 0.80, E is 35.7GPa.

Under action of strain energy, roof and sidewall may be damaged. Assuming that the released strain energy causes a crack of length a and b on roof and sidewall respectively. Energy absorbed by the crack on roof and sidewall is calculated by Eq. (10). The γ represents the energy consumed per unit area, which is calculated by Eq. (11).

$$\begin{cases} U_{Roof} = 2a\gamma \\ U_{Sidewall} = 2b\gamma \end{cases} \tag{10}$$

$$\gamma = \frac{\int_0^l F dl}{2A} \tag{11}$$

By specimen testing made from surrounding rock of the mine, it is obtained that γ is about 1.2 KJ/m^2 in Brazilian split test, and is about 7.1 KJ/m^2 in uniaxial compression test. $U_{T\text{-}Roof}$ is used to represent the strain energy required to form a tensile crack on roof. $U_{T\text{-}Sidewall}$ is the strain energy required to produce a tensile crack on sidewall. $U_{S\text{-}Roof}$ is used to represent the strain energy required to form a shear crack on roof. $U_{S\text{-}Sidewall}$ is the strain energy required to produce a shear crack on sidewall, which is shown in Eq. (13) and (14).

$$\begin{cases} U_{e-Roof} = 0.178(0.0266h)^2, KJ/m \\ U_{e-Sidewall} = 0.163(0.0461h - 7.11)^2, KJ/m \end{cases} \tag{12}$$

$$\begin{cases} U_{T-Roof} = 10.8, KJ/m \\ U_{T-Sidewall} = 10.3, KJ/m \end{cases} \tag{13}$$

$$\begin{cases} U_{S-Roof} = 63.9, KJ/m \\ U_{S-Sidewall} = 61.1, KJ/m \end{cases} \tag{14}$$

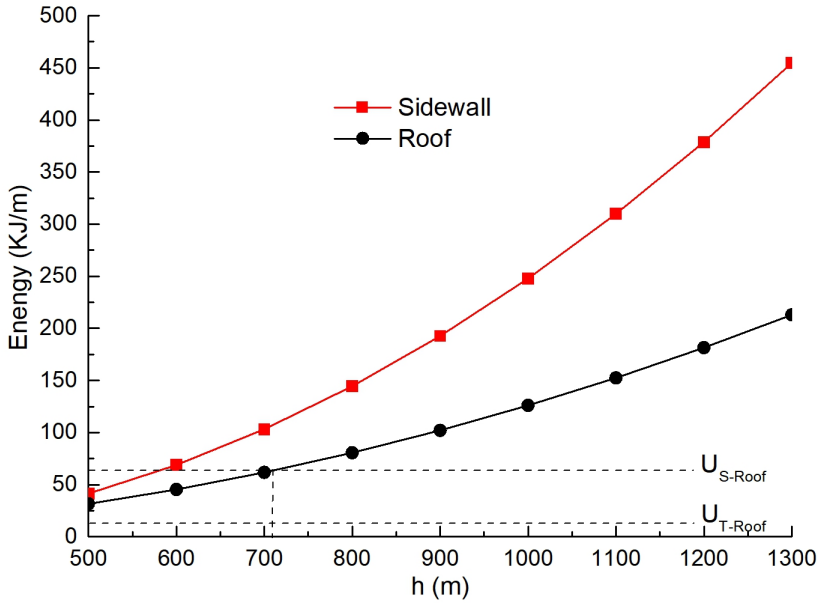

Fig. 13 Strain energy released of roof and sidewall at different buried depths

As shown in Fig. 13, strain energy released of roof and sidewall in the mine increases rapidly with depth. It can be seen from Eq. (9) that strain energy released increases with the second power of buried depth. The rapid growth of strain energy released in deep can cause failure to surrounding rock. For example, as shown in Fig. 14, a large number of rock spalling and cracks are produced in sidewall of roadway with buried depth of 720m. It shows that the strain energy released of surrounding rock at this buried depth cannot be ignored. In addition, strain energy released grows faster and faster with depth, and strain energy released of sidewall at 1000 m is 6 times that at 500 m. This is also the reason why spalling occurred at buried depth of 745m in Table 1 and Fig. 1-4, while rockburst and large-area collapse occurred at buried depth of 980m and deeper.

Therefore, the release of strain energy of surrounding rock after excavation should be paid attention in the mine. In deep engineering, high-strength rock bolts often suffer brittle fracture, and high energy-absorbing materials are more suitable for surrounding rock support than pure high-strength materials. Adopting energy-absorbing support methods to absorb the released strain energy of surrounding rock can achieve good results, which is also a view that scholars increasingly agree [18, 37].

Fig. 14 A large number of rock spalling and cracks produced in sidewall of roadway with buried depth of 720m

4. Application: roadway support with energy absorbing material

After excavation of deep roadway in the mine, there are often ground pressure disasters such as the rockburst, spalling, large-area collapse roof sinking and deformation of surrounding. The problem can be solved from the perspective of strain energy release of surrounding rock.

Taking a roadway with depth of 1000m of the mine as an example, the released strain energy by roof and sidewall are 126 KJ/m and 248 KJ/m respectively. In order to absorb released strain energy, energy-absorbing materials are used for supporting design. Taking a kind of energy-absorbing anchor as an example, the maximum absorbed energy of a single anchor is about 67.2KJ [16]. Studies have shown that when the safety factor reaches 1.15, the spalling probability of surrounding rock is basically zero, and when safety factor is 0.85, only very minor spalling will occur [34]. Therefore, safety factor of roof and floor plates is set to 1.15, and the safety factor of 0.85 is selected for sidewalls because of the excessive strain energy. The strain energy that supporting structure needs to absorb is calculated by Eq. (15).

In terms of support design, the row spacing of rock bolts is set to 1m, which means that each row of bolts needs to absorb the released energy by surrounding rock within a length of 1m. Rock bolts arranged in different positions should be able to absorb the strain energy released by corresponding position of surrounding rock. The number of rock bolts required for roof is

$1.15\times126KJ/67.2KJ$, which is about 2, and the number of rock bolts required for sidewall is $0.85\times248KJ/67.2KJ$, which is about 3. The floor also needs 2 bolts, and another sidewall needs 3 bolts. The bottom of rock bolts is connected by steel net, and the final support design is shown in Fig. 15.

$$U_{s-Support} \geq (1.15U_{e-Roof} + 1.15U_{e-Floor} + 2\times0.85U_{e-Sidewall}) \quad (15)$$

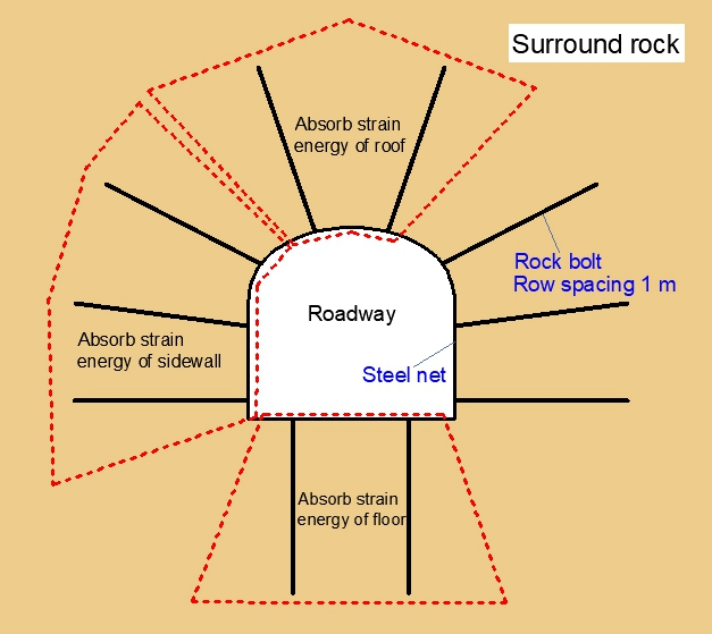

Fig. 15 Support design using energy-absorbing bolts to absorb strain energy released of surrounding rock

5. Conclusion

Main conclusions of this paper are as follows:

(1) Through field investigation, it is found that the degree and number of ground pressure disasters in Xincheng Gold Mine increase significantly with depth. The slabbing of surrounding rock starts from buried depth of 745m, spalling of surrounding rock and rock bolt fall off from buried depth of 830m, and rockburst and large-area of collapse from buried depth of 980m.

(2) When the maximum tangential stress between 0.4-0.6 times the uniaxial compressive strength, surrounding rock in the mine is prone to local spalling failure. When maximum tangential stress is greater than 0.6 times uniaxial compressive strength, surrounding rock in the mine is prone to serious failure, such as rockbursts and large-scale collapses.

(3) After excavation, the rebound strain and displacement of surrounding rock in the mine increases linearly with buried depth, and the strain energy released of surrounding rock increases rapidly with the second power of buried depth. The rapidly increasing strain energy released is main reason why deep ground pressure disasters are becoming more and more serious.

(4) In terms of surrounding rock support, energy-absorbing materials such as energy-absorbing bolts can well absorb the strain energy released of surrounding rock in the mine. As shown in Eq. (15) and Fig. 15, rock bolts arranged in different positions should be able to absorb strain energy released by corresponding position of surrounding rock.

Acknowledgments

The authors would like to thank the financial support from the National Natural Science Foundation of China (No. 51774321) and the State Key Research Development Program of China (No. 2018YFC0604606).

Author contributions

Peng Xiao completed the field investigation, theoretical analysis and manuscript writing; Guoyan Zhao provided the theoretical analysis method; Huanxin Liu provided some figures and engineering background information.

Competing interests

The authors declare no competing interests.

References

[1] Li X, Gong F, Wang S, et, al. Coupled static-dynamic loading mechanical mechanism and dynamic criterion of rockburst in deep hard rock mines. Chinese Journal of Rock Mechanics and Engineering. 2019;38(4):708-723.

[2] Miao S, Cai M, Guo Q, huang Z. Rock burst prediction based on in-situ stress and energy accumulation theory. International Journal of Rock Mechanics & Mining Sciences. 2016;83:86-94.

[3] Li P, Cai M, Guo Q, Miao S. In Situ Stress State of the Northwest Region of the Jiaodong Peninsula, China from Overcoring Stress Measurements in Three Gold Mines. Rock Mechanics and Rock Engineering. 2019;52:4497-4507.

[4] Heidbach O, Rajabi M, Cui X, Fuchs K, Mueller B, Reinecker J, et al. The World Stress Map database release 2016: Crustal stress pattern across scales. Tectonophysics. 2018;744:484-98.

[5] Palmstrom A, Broch E. Use and misuse of rock mass classification systems with particular reference to the Q-system.

Tunnelling And Underground Space Technology. 2006;21:575-93.
[6] Pantelidis L. Rock slope stability assessment through rock mass classification systems. International Journal Of Rock Mechanics And Mining Sciences. 2009;46:315-25.
[7] Liu Z, Dang W. Rock quality classification and stability evaluation of undersea deposit based on M-IRMR. Tunnelling and Underground Space Technology. 2014;40:95-101.
[8] Li D, Xiao P, Han Z, Zhu Q. Mechanical and failure properties of rocks witha cavity under coupled static and dynamic loads. Engineering Fracture Mechanics. 2020;225:106195.
[9] Qiu J, Li X, Li D, Zhao Y, Hu C, Liang L. Physical Model Test on the Deformation Behavior of an Underground Tunnel Under Blasting Disturbance. Rock Mechanics and Rock Engineering. 2020.
[10] Xiao P, Li D, Zhao G, Zhu Q, Liu H, Zhang C. Mechanical properties and failure behavior of rock with different flaw inclinations under coupled static and dynamic loads. Journal of Central South University. 2020;27:2945-58.
[11] Yang S-Q, Hu B. Creep and permeability evolution behavior of red sandstone containing a single fissure under a confining pressure of 30MPa. Scientific Reports. 2020;10.
[12] Labuz J, Zang A. Mohr-Coulomb failure criterion. Rock Mech Rock Eng. 2012;45:975-59.
[13] Si X, Gong F, Li X, Wang S, Luo S. Dynamic Mohr-Coulomb and Hoek-Brown strength criteria of sandstone at high strain rates. International Journal Of Rock Mechanics And Mining Sciences. 2019;115:48-59.
[14] Shen B, Shi J, Barton N. An approximate nonlinear modified Mohr-Coulomb shear strength criterion with critical state for intact rocks. Journal Of Rock Mechanics And Geotechnical Engineering. 2018;10:645-52.
[15] Li CC. A new energy-absorbing bolt for rock support in high stress rock masses. International Journal of Rock Mechanics & Mining Sciences. 2010;47:396-404.
[16] He M, Guo Z. Mechanical Property and Engineering Application of Anchor Bolt with Constant Resistance and Large Deformation. Chinese Journal of Rock Mechanics and Engineering. 2014;33:1297-308.
[17] Ansell A. Laboratory testing of a new type of energy absorbing rock bolt. Tunnelling And Underground Space Technology. 2005;20:291-300.
[18] He M, Gong W, Wang J, Qi P, Tao Z, Du S, et al. Development of a novel energy-absorbing bolt with extraordinarily large elongation and constant resistance. International Journal Of Rock Mechanics And Mining Sciences. 2014;67:29-42.
[19] Cai W, Chang Z, Zhang D, Wang X, Cao W, Zhou Y. Roof filling control technology and application to mine roadway damage in small pit goaf. International Journal of Mining Science and Technology. 2019;29:477-82.
[20] Rong K, Lan W, Li H. Industrial Experiment of Goaf Filling Using the Filling Materials Based on Hemihydrate Phosphogypsum. Minerals. 2020;10.
[21] Abdelhadi K, Latifa O, Khadija B, Lahcen B. Valorization of mining waste and tailings through paste backfilling solution, Imiter operation, Morocco. International Journal of Mining Science And Technology. 2016;26:511-6.
[22] Zhang J, Liu L, Zhang F, Cao J. Development and application of new composite grouting material for sealing groundwater inflow and reinforcing wall rock in deep mine. Scientific Reports. 2018;8.
[23] Zhang C, Pu C, Cao R, Jiang T, Huang G. The stability and roof-support optimization of roadways passing through unfavorable geological bodies using advanced detection and monitoring methods, among others, in the Sanmenxia Bauxite Mine in China's Henan Province. Bulletin Of Engineering Geology And the Environment. 2019;78:5087-99.
[24] Liu DJ, Zuo JP, Wang J, Zhang TL, Liu HY. Large deformation mechanism and concrete-filled steel tubular support control technology of soft rock roadway-A case study. Engineering Failure Analysis. 2020;116.
[25] Huang WP, Yuan Q, Tan YL, Wang J, Liu GL, Qu GL, et al. An innovative support technology employing a concrete-filled steel tubular structure for a 1000-m-deep roadway in a high in situ stress field. Tunnelling And Underground Space Technology. 2018;73:26-36.
[26] Dong L, Zou W, Li X, Shu W, Wang Z. Collaborative localization method using analytical and iterative solutions for microseismic/acoustic emission sources in the rockmass structure for underground mining. Engineering Fracture

Mechanics. 2019;210:95-112.
[27] Lu C-P, Liu G-J, Zhang N, Zhao T-B, Liu Y. Inversion of stress field evolution consisting of static and dynamic stresses by microseismic velocity tomography. International Journal Of Rock Mechanics And Mining Sciences. 2016;87:8-22.
[28] Niu W-j, Feng X-T, Xiao Y-x, Feng G-l, Yao Z-b, Hu L. Identification of potential high-stress hazards in deep-buried hard rock tunnel based on microseismic information: a case study. Bulletin Of Engineering Geology And the Environment. 2020.
[29] He M, R. Leal eS, Andre M, E V, LRE S, C X. Analysis of excessive deformations in tunnels for safety evaluation. Tunnelling And Underground Space Technology. 2015;45:190-202.
[30] Wu Z, Wu S, Cheng Z. Discussion and application of a risk assessment method for spalling damage in a deep hard-rock tunnel. Computers and Geotechnics. 2020;124.
[31] Eskesen SD, Tengborg P, Kampmann J, Veicherts TH. Guidelines for tunnelling risk management: International Tunnelling Association, Working Group No.2. Tunnelling And Underground Space Technology. 2004;19:217-37.
[32] Gong F, Wu W, Li T, Si X. Experimental simulation and investigation of spalling failure of rectangular tunnel under different three-dimensional stress states. International Journal of Rock Mechanics and Mining Sciences. 2019;122.
[33] Read R. 20 years of excavation response studies at AECL's Underground Research Laboratory. International Journal of Rock Mechanics and Mining Sciences. 2004;41:1251-75.
[34] Martin CD, Christiansson R. Estimating the potential for spalling around a deep nuclear waste repository in crystalline rock. International Journal of Rock Mechanics & Mining Sciences. 2009;46:219-28.
[35] Li D, Li CC, Li X. Influence of Sample Height-to-Width Ratios on Failure Mode for Rectangular Prism Samples of Hard Rock Loaded In Uniaxial Compression. Rock Mechanics & Rock Engineering. 2010;44:253-67.
[36] Li D, Li X, Li CC. Experimental Studies of Mechanical Properties of Two Rocks Under Direct Compression and Tension. Chinese Journal of Rock Mechanics and Engineering. 2010;29:624-32.
[37] Li CC. Performance of D-bolts Under Static Loading. Rock Mechanics And Rock Engineering. 2012;45:183-92.

Figures

Figure 1

Mining depth 745m

Figure 2

Mining depth 830m

Figure 3

Mining depth 930m

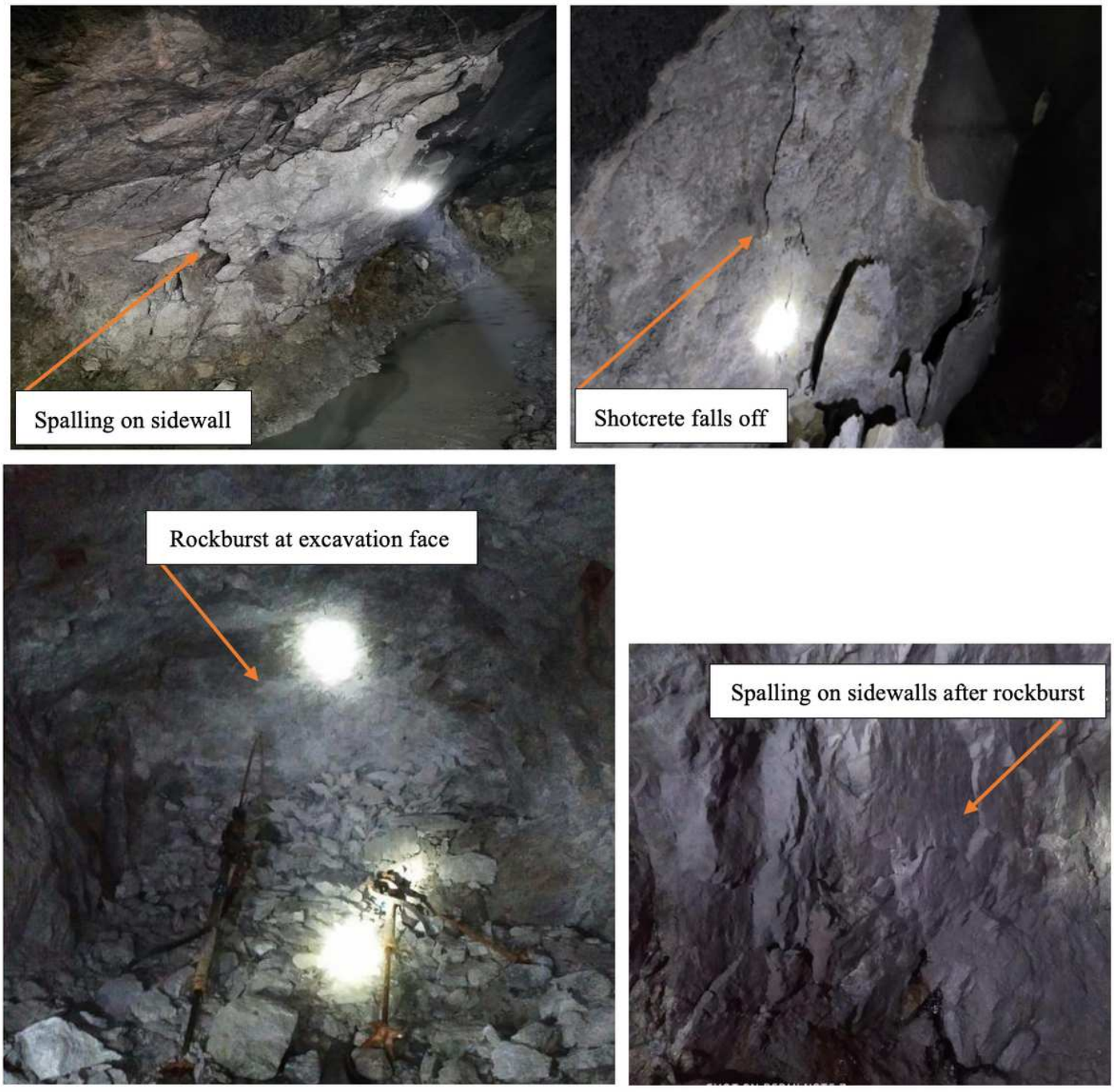

Figure 4

Mining depth 980m

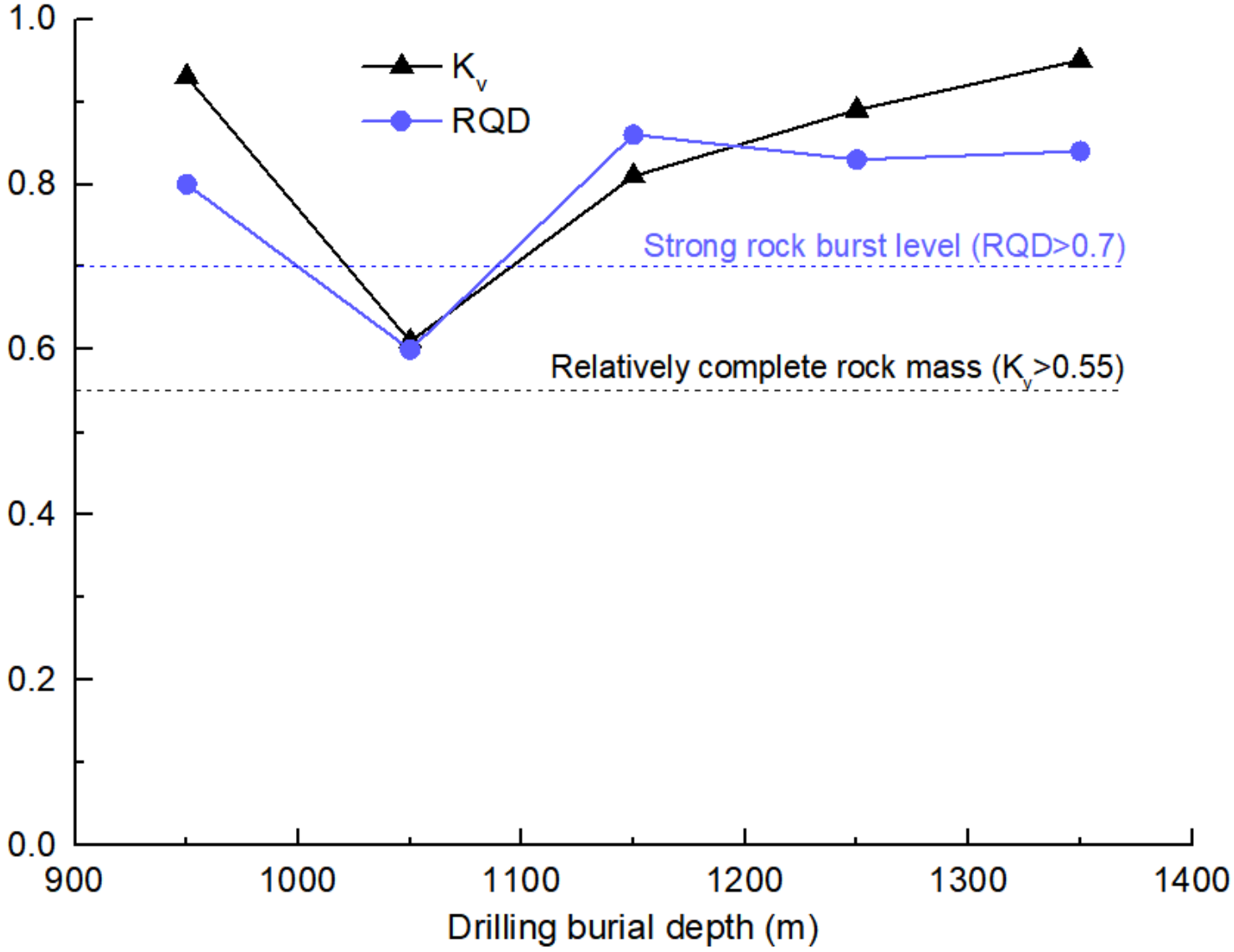

Figure 5

RQD and Kv values of surrounding rock at different buried depths of the mine

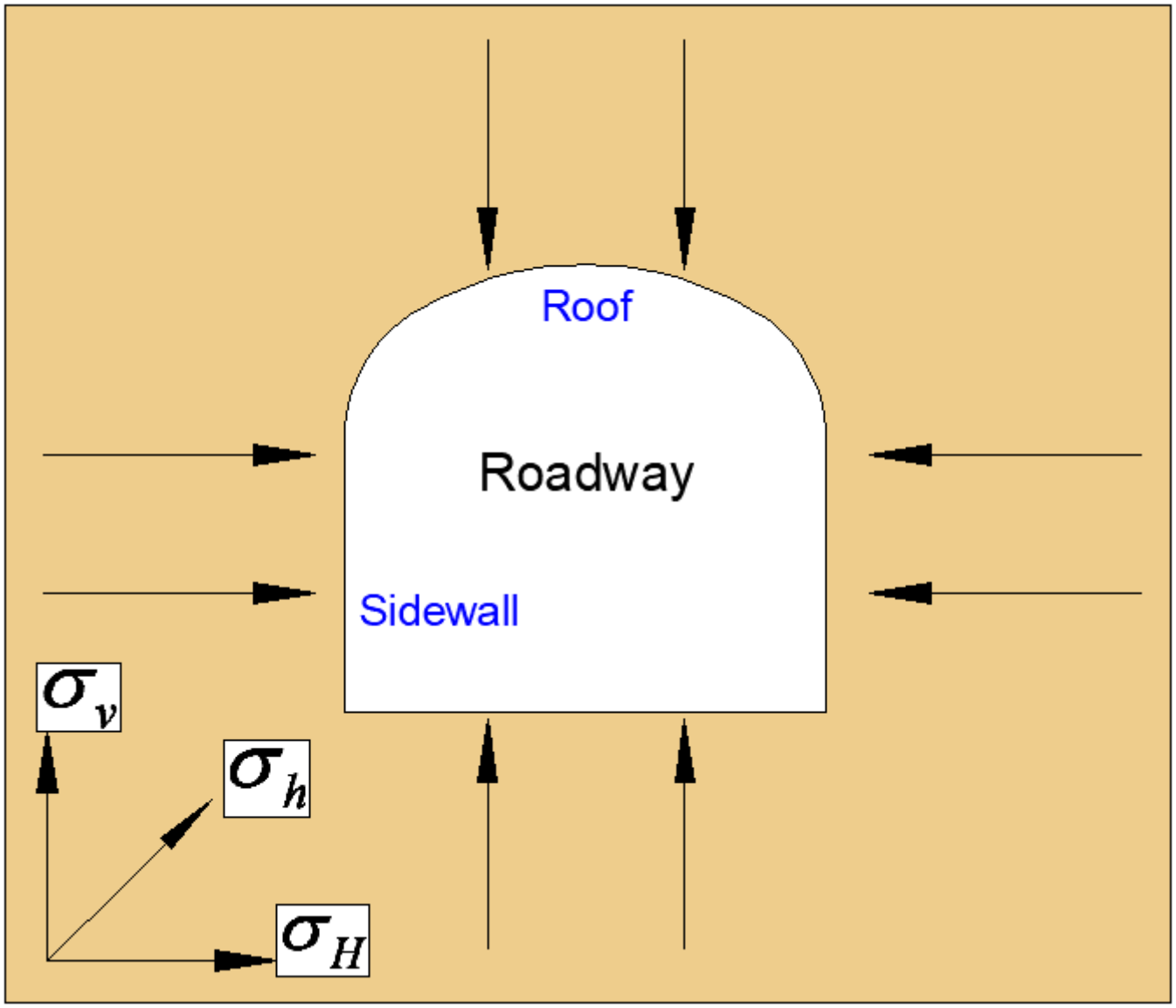

Figure 6

Stress state of the horizontal transportation roadway

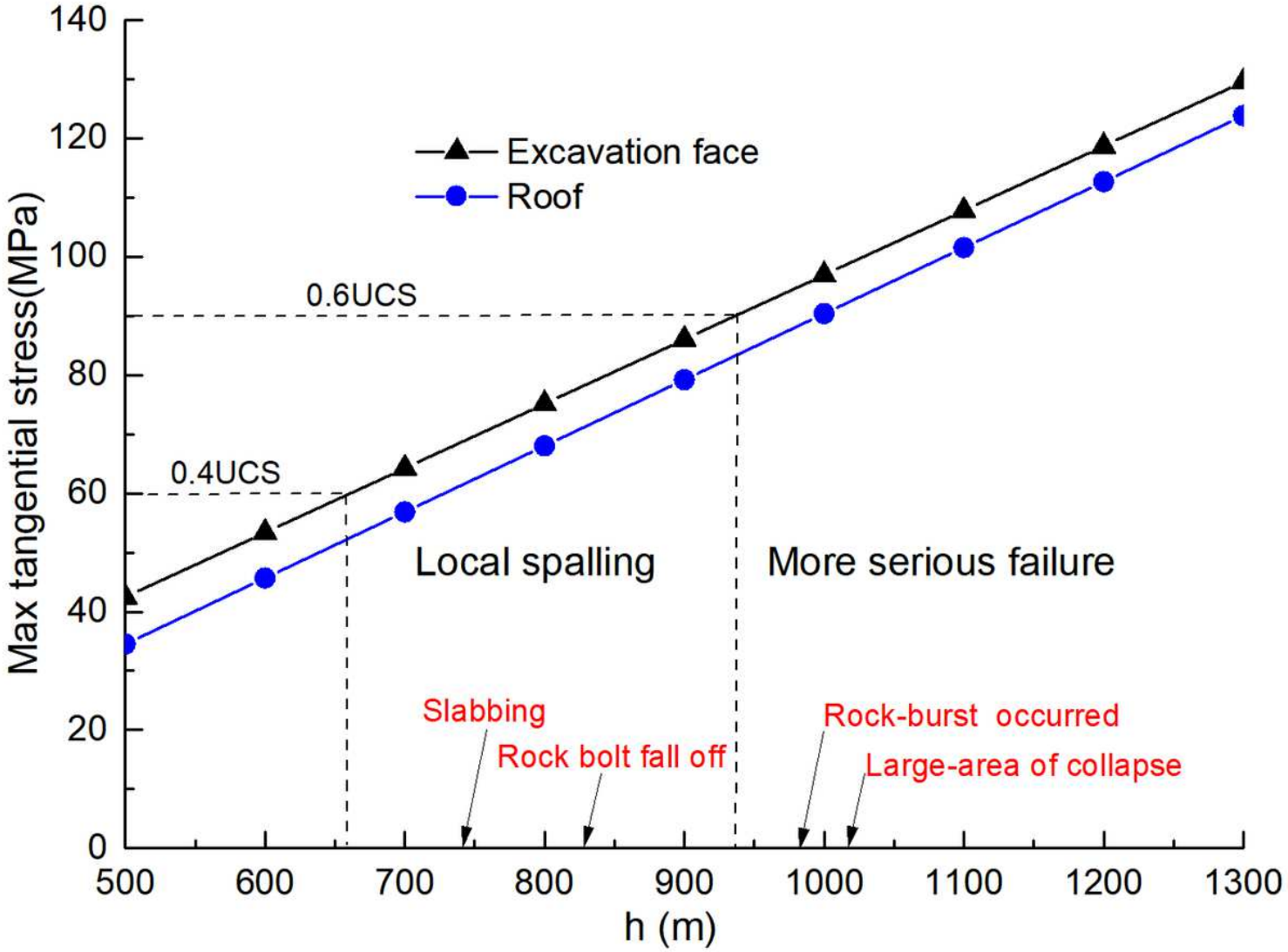

Figure 7

Maximum tangential stress of roadways at different buried depth

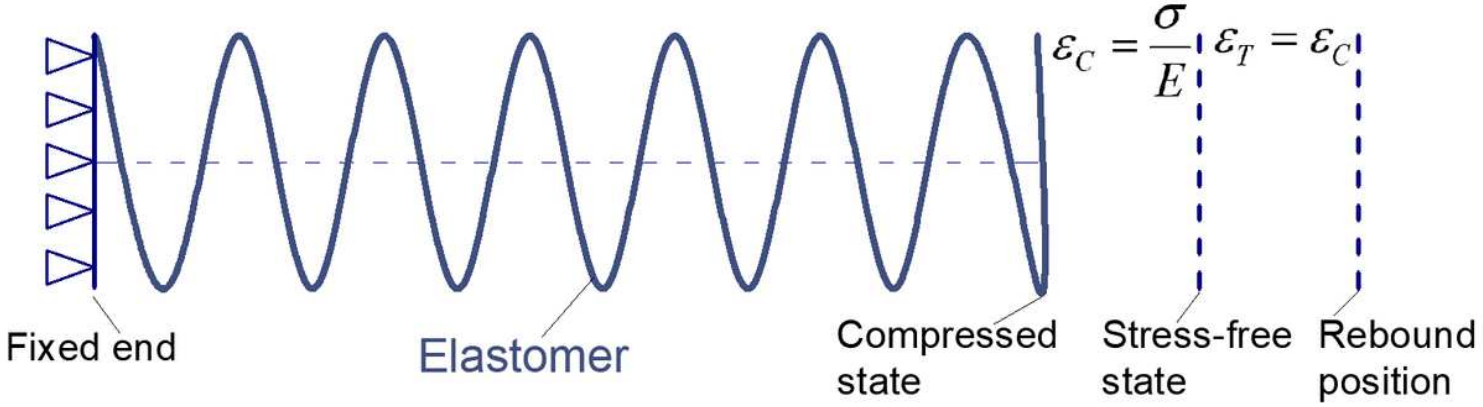

Figure 8

Strain rebound process of elastomer after stress relief

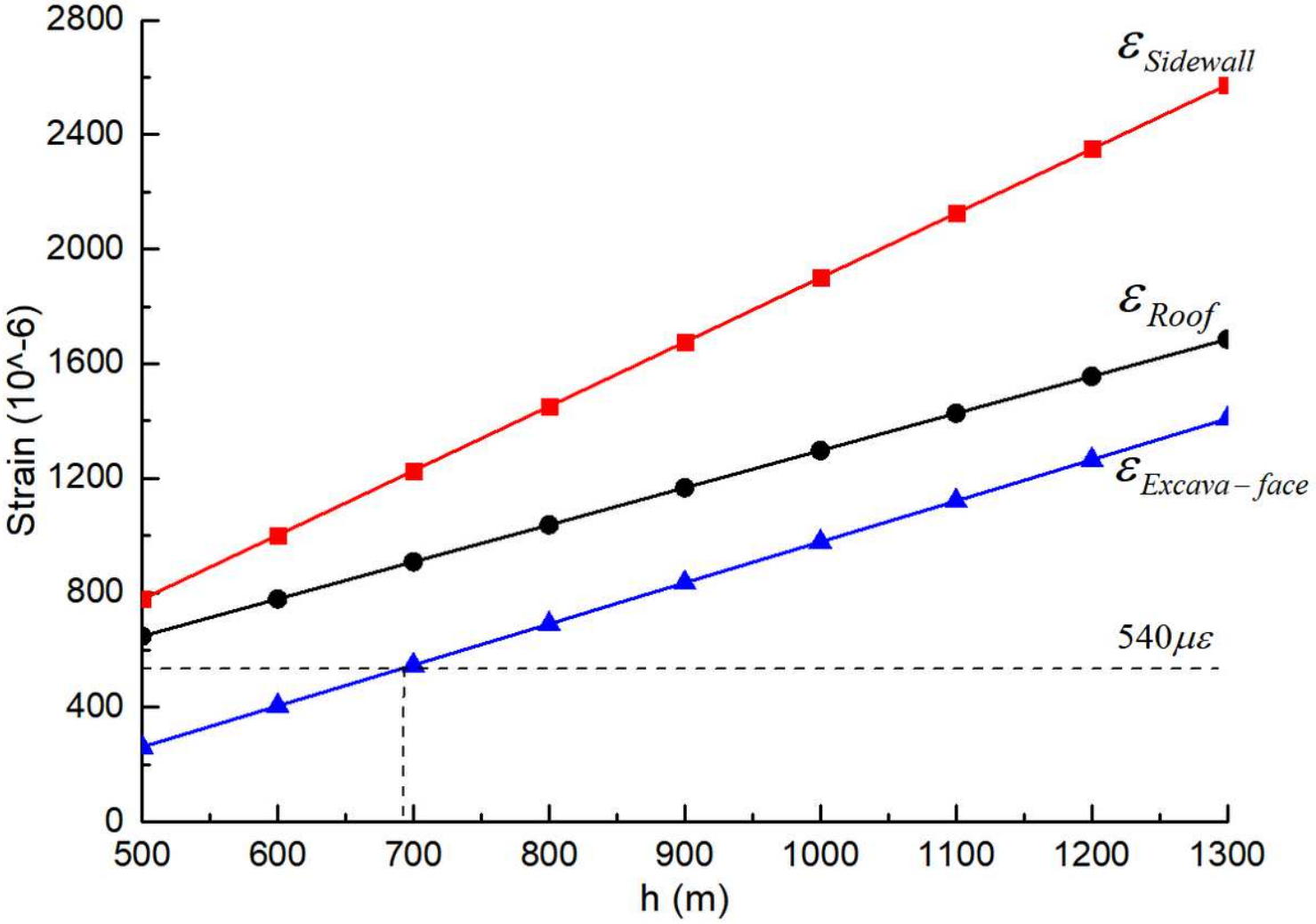

Figure 9

Rebounded strain of sidewall, roof and excavation surface of roadway at different buried depths

Figure 10

Large deformation of sidewall in a soft rock roadway

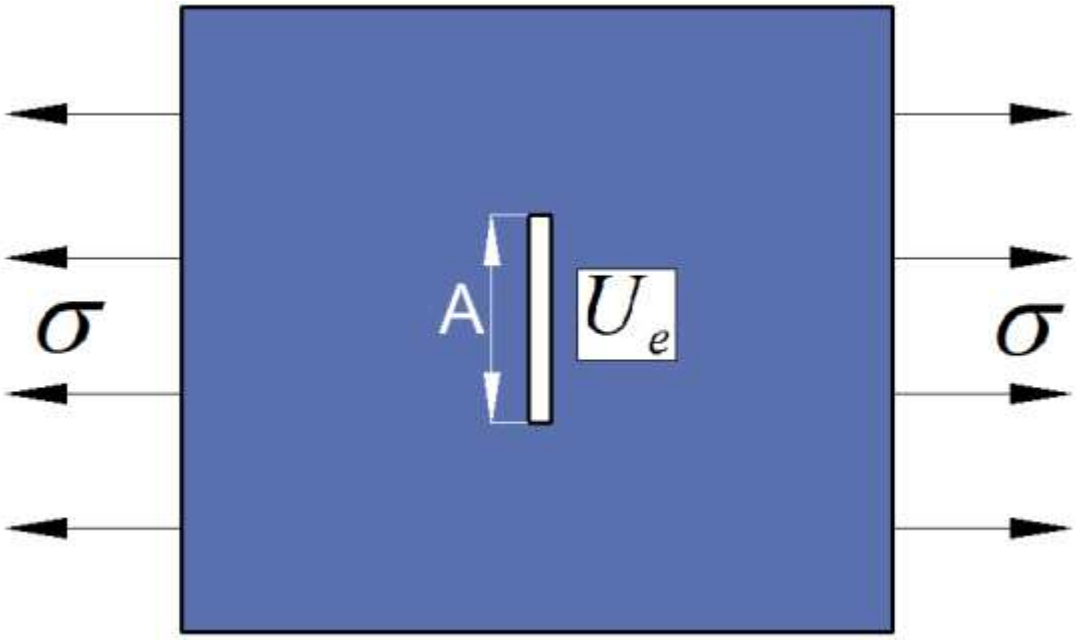

Figure 11

The elastic plate subjected to uniform stress is cut with a crack with area A

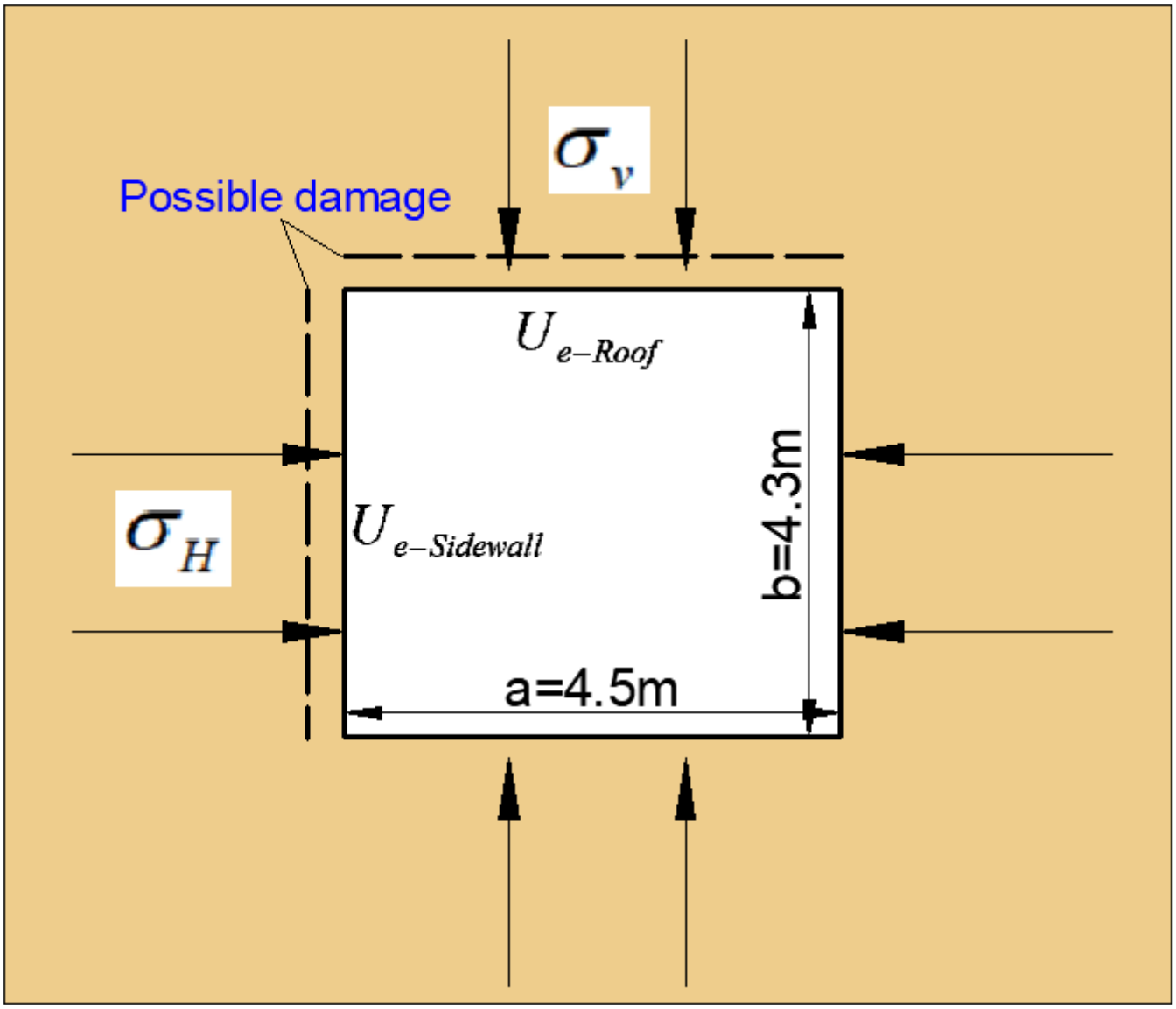

Figure 12

Strain energy released after roadway excavation and possible damage

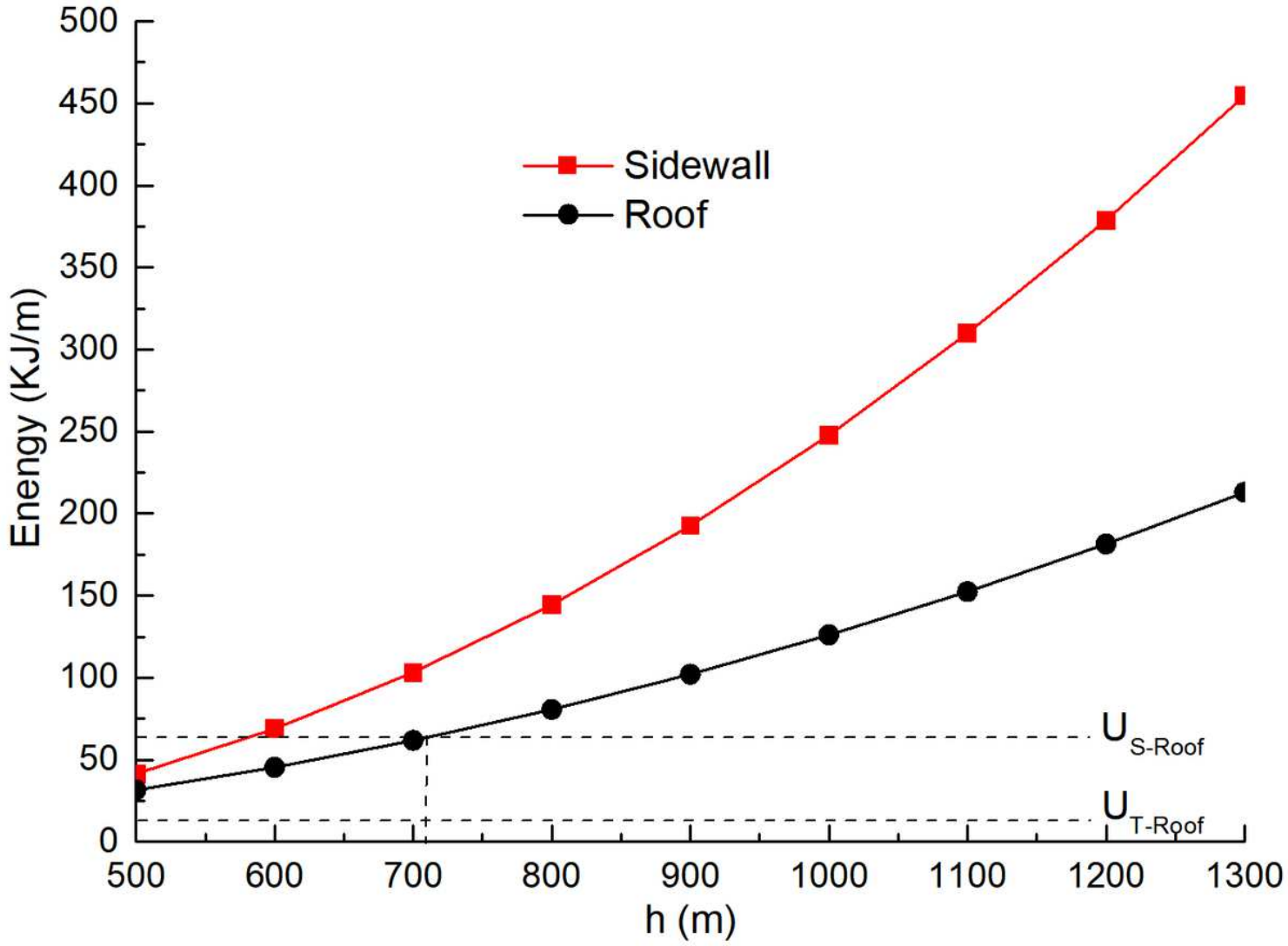

Figure 13

Strain energy released of roof and sidewall at different buried depths

Figure 14

A large number of rock spalling and cracks produced in sidewall of roadway with buried depth of 720m

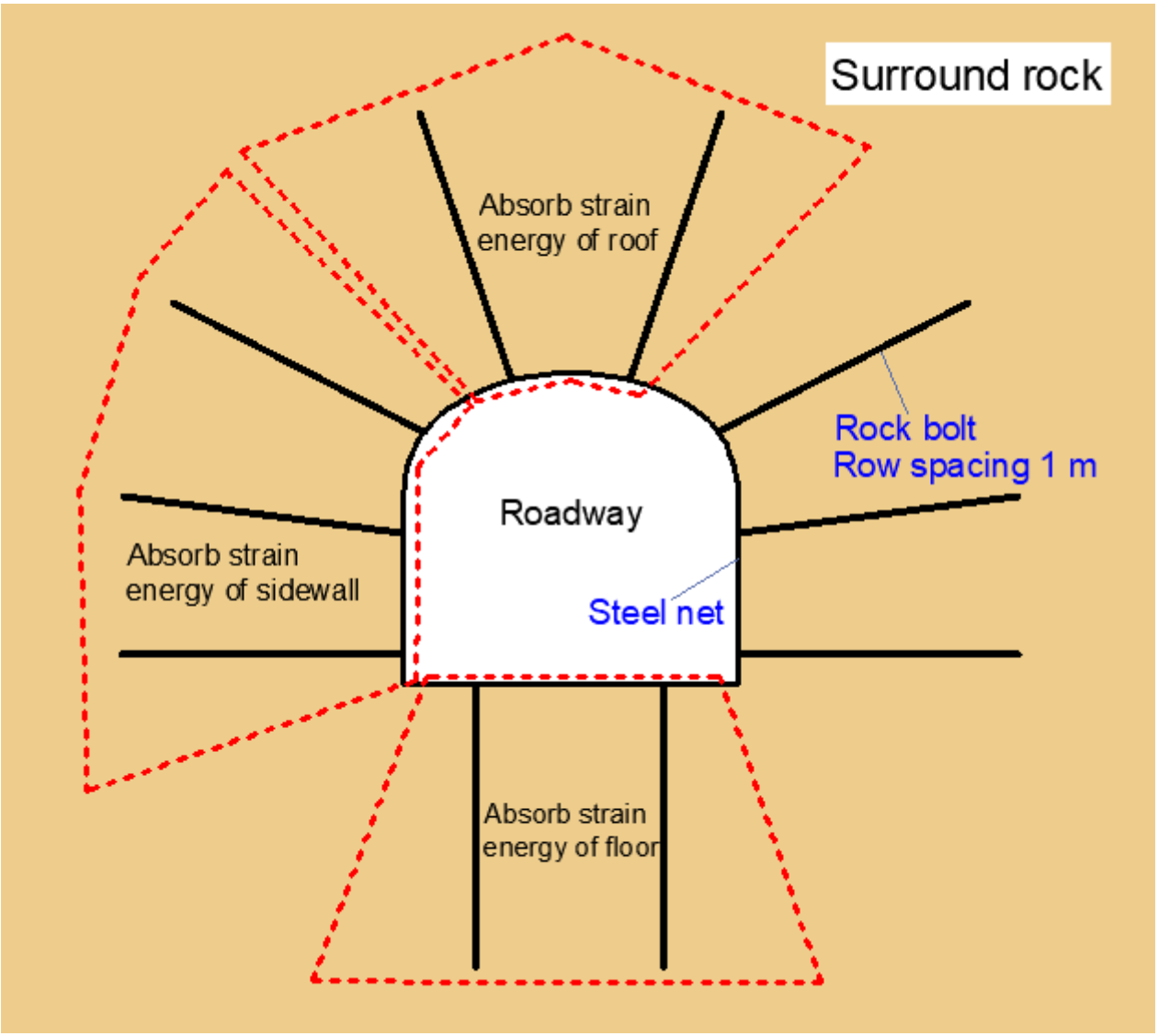

Figure 15

Support design using energy-absorbing bolts to absorb strain energy released of surrounding rock